Isotropy or weak vertical transverse isotropy in D″ beneath the Atlantic Ocean

Edward J. Garnero and Melissa M. Moore
Department of Geological Sciences, Arizona State University, Tempe, Arizona, USA

Thorne Lay
Earth Sciences Department and Institute of Geophysics and Planetary Physics, University of California, Santa Cruz, California, USA

Matthew J. Fouch
Arizona State University, Department of Geological Sciences, Tempe, Arizona, USA

Received 30 January 2004; revised 14 May 2004; accepted 14 June 2004; published 13 August 2004.

[1] Shear velocity properties of D″ beneath the central Atlantic Ocean are explored using predominantly European seismic recordings of intermediate and deep focus (>100 km) South American earthquakes. Broadband data are analyzed and, when possible, corrected for upper mantle models of receiver-side anisotropic structure. Regional shear velocity heterogeneity in D″ is mapped by analysis of 306 *S-SKS* differential times that have been corrected for three-dimensional seismic velocity structure above D″ using a whole mantle tomographic model. This correction yields modest (less than ±2%) estimates of seismic velocity heterogeneity in D″, with a transition from high to low seismic velocities traversing from west to east beneath the central Atlantic, in agreement with global tomographic models. Additionally, shear wave splitting of S and S_{diff} for the same recordings was analyzed to assess seismic anisotropy in D″. The highest-quality data provide 105 splitting times between *SH* and *SV* onsets that are mostly within the ±1 s uncertainty level. The few larger values generally exhibit *SV* delayed relative to *SH*. Assuming an anisotropy geometry involving vertical transverse isotropy (VTI), as preferred in most regions of D″ that have been studied to date, <0.5% anisotropy strength within a 100 km thick layer, or <0.25% anisotropy within a 300 km thick layer are compatible with the data. These values are low in comparison to those found in high-velocity regions beneath the circum-Pacific Ocean or in the low-velocity region beneath the central Pacific, and many observations are, in fact, consistent with isotropic structure. The lack of strong VTI relative to other regions may be due to (1) the absence of stress from overlying midmantle downwelling, (2) relatively weaker shear flow in the D″ boundary layer, and/or (3) lack of chemical heterogeneity that could develop either lattice-preferred orientation or shape-preferred orientation. The azimuthal sampling of this region of D″ is quite limited; thus the precise geometry and mechanism of any anisotropy are difficult to constrain. It remains possible that this region may contain subtle azimuthal anisotropy that could couple the *SV* and *SH* signals; however, amplitude observations suggest that any such coupling is minor. *INDEX TERMS:* 7203 Seismology: Body wave propagation; 7207 Seismology: Core and mantle; 7260 Seismology: Theory and modeling; 3909 Mineral Physics: Elasticity and anelasticity; 3902 Mineral Physics: Creep and deformation; *KEYWORDS:* anisotropy, lower mantle, core-mantle boundary

Citation: Garnero, E. J., M. M. Moore, T. Lay, and M. J. Fouch (2004), Isotropy or weak vertical transverse isotropy in D″ beneath the Atlantic Ocean, *J. Geophys. Res.*, *109*, B08308, doi:10.1029/2004JB003004.

1. Introduction

[2] The lowermost mantle has long been of interest due to its anomalous seismological properties relative to the overlying mantle. It is widely accepted that understanding the characteristics of the boundary layer at the base of the mantle is critical to resolving issues concerning large-scale dynamics of the Earth. The lowermost several hundred kilometers of the mantle, called the D″ region [*Bullen*, 1949], are characterized as having strong thermal, chemical, and dynamical variability and this region likely plays an

0148-0227/04/2004JB003004$09.00

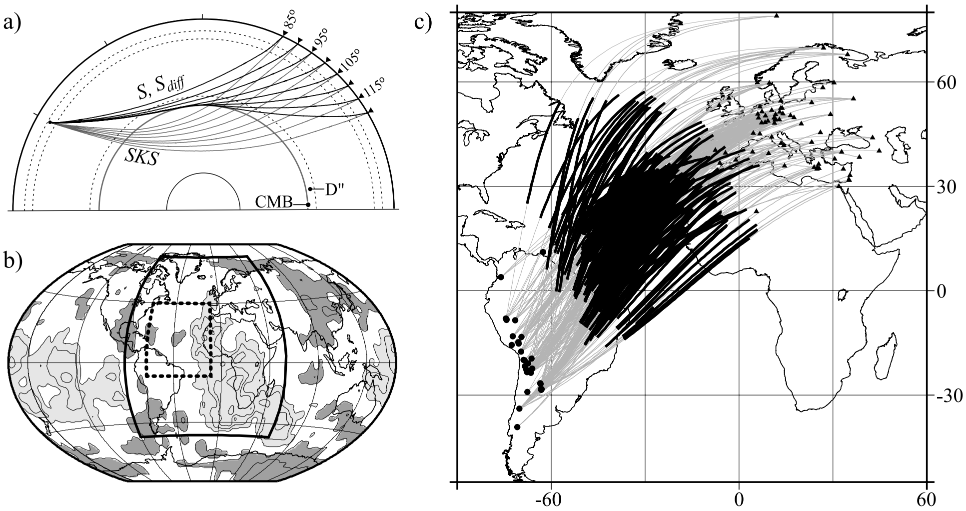

Figure 1. (a) Seismic ray paths of the *S* (or S_{diff}) and *SKS* phase pair used in this study for a 500 km deep earthquake. (b) Shear velocity heterogeneity at the base of the mantle for the *Grand* [2002] model. The region between $-1\% < \delta V_S < +1\%$ is white, and high- and low-velocity regions with heterogeneity amplitudes greater than this region are dark and lightly shaded, respectively, with contour lines drawn at every 1%. The larger box region is shown in Figure 1c. (c) Events (circles), stations (triangles), great circle paths (lightly shaded lines), and the PREM-predicted sampling for a 250 km thick D″ layer (thicker black lines). The thick dashed line area in Figure 1b corresponds to the geographical region shown in Figure 5.

important role in mantle dynamics [e.g., *Lay et al.*, 1998a; *Wysession et al.*, 1998; *Kendall*, 2000; *Garnero*, 2000; *Karato*, 2003; *Lay and Garnero*, 2004; *Lay et al.*, 2004; *Jellinek and Manga*, 2004]. Over the past decade our understanding of D″ has significantly improved as a result of numerous studies of deep mantle shear wave splitting (e.g., see reviews by *Lay et al.* [1998b] and *Kendall* [2000]). This is typically observed as relative arrival time difference of the horizontally and vertically polarized components of shear waves; *SH* and *SV*, respectively. Shear wave splitting occurring in D″ is typically measured for the seismic phases *ScS*, *S*, or diffracted *S* (S_{diff}), and in this study we focus on the latter two arrivals (see Figure 1a). The majority of past splitting observations have *SH* component arrivals 1–6 s earlier than *SV* component arrivals, with little indication of coupling between the components (e.g., see summaries of *Lay et al.* [1998b], *Kendall* [2000], and *Moore et al.* [2004]). This observation is most simply explained by the presence of vertical transverse isotropy (VTI) in D″, such as would result from material with hexagonal symmetry with a vertical symmetry axis or from horizontal layering of high- and low-velocity lamellae [*Karato*, 1998; *Kendall*, 2000; *Karato and Karki*, 2001; *Moore et al.*, 2004]. VTI in D″ will not affect *SKS* waveforms or other purely polarized waves traversing the region.

[3] To date, most research on shear wave splitting and anisotropy in D″ has involved regions that have either high shear velocities [*Mitchell and Helmberger*, 1973; *Lay and Helmberger*, 1983; *Lay and Young*, 1990, 1991; *Kendall and Silver*, 1996; *Matzel et al.*, 1996; *Ding and Helmberger*, 1997; *Garnero and Lay*, 1997; *Fouch et al.*, 2001; *Thomas and Kendall*, 2002; *Thomas et al.*, 2002; *Garnero and Lay*, 2003; *Rokosky et al.*, 2004] or low shear velocities [*Vinnik et al.*, 1995; *Kendall and Shearer*, 1995; *Pulliam and Sen*, 1998; *Ritsema et al.*, 1998; *Russell et al.*, 1998; *Vinnik et al.*, 1998; *Russell et al.*, 1999; *Ritsema*, 2000; *Fouch et al.*, 2001], relative to standard reference Earth models. high-velocity D″ regions tend to underlie areas of present or past subduction, while low-velocity regions tend to underlie groupings of surface hot spots and related mantle upwellings [e.g., *Morgan*, 1971; *Hager et al.*, 1985; *Ribe and Devalpine*, 1994; *Grand et al.*, 1997; *Thorne et al.*, 2004]. When comparing maps of D″ anisotropy to tomographic images, one generally finds a weak correlation between *S* velocity anomalies (δV_S) and the strength of anisotropy [e.g., *Lay et al.*, 1998b; *Garnero and Lay*, 2003; *Rokosky et al.*, 2004]; however, it is possible that the fundamental cause of anisotropy is different between high- and low-velocity regions [e.g., *McNamara et al.*, 2002]. The origin of D″ velocity heterogeneity may be thermal, chemical, or mineralogical, and its relationship to anisotropy remains unclear [e.g., *Lay et al.*, 2004].

[4] The study region in this paper differs from previous work in that the regional seismic velocities imaged by seismic tomography are transitional, characterized by a west-to-east trend of decreasing velocity with an overall average close to values of standard Earth models (Figure 1b) [e.g., *Masters et al.*, 2000; *Grand*, 2002]. Our data straddle this transition zone, allowing us to seek systematic relationships between velocity structure and anisotropy. We quantify the regional patterns of shear velocity heterogeneity, using differential travel time analysis of *S-SKS*, and D″ anisotropy, using shear wave splitting measurements of *S*(*SV*)-*S*(*SH*). Throughout this paper we use *S* to denote both *S* and S_{diff} phases. Differential times between *S* and *SKS* (*S-SKS*) suppress contributions from upper mantle heterogeneity and also reduce possible effects of source mislocation and origin time errors. It is necessary, however, to properly

Table 1. Events Used in This Study[a]

Date	Depth, km	Latitude, deg	Longitude, deg.
23 June 1991	558	−26.80	−63.35
6 July 1991	104.	−13.11	−72.19
16 April 1992	122.	−20.00	−68.48
6 May 1993	572.	−8.47	−71.49
19 Oct. 1993	272.	−22.38	−65.97
10 Jan. 1994	596.	−13.34	−69.45
29 April 1994	561.	−28.30	−63.25
10 May 1994	600.	−28.50	−63.10
16 June 1994	199.	−15.25	−70.29
19 Aug. 1994	563.	−26.64	−63.42
11 Nov. 1994	120.	−15.63	−72.54
7 Dec. 1994	235.	−23.42	−66.64
12 Dec. 1994	148.	−17.48	−69.60
10 Feb. 1995	118.	−19.94	−68.76
14 Feb. 1995	147.	−23.37	−67.69
3 April 1998	164.	−8.15	−74.24
8 Oct. 1998	136.	−16.12	−71.40
15 Sept. 1999	218.	−20.93	−67.28
23 April 2000	608.	−28.31	−62.99
12 May 2000	225.	−23.55	−66.45
16 June 2000	120.	−33.88	−70.09
4 Oct. 2000	110.	11.12	−62.56
1 Nov. 2000	150.	−7.95	−74.42
21 April 2001	127.	−29.10	−67.52
19 June 2001	146.	−22.74	−67.88
29 June 2001	273.	−19.52	−66.25
22 Sept. 2001	178.	3.87	−75.97
28 March 2002	125.	−21.66	−68.33

[a]From USGS catalog.

account for deeper mantle velocity heterogeneity above the D″ region of interest, and we do this using an aspherical mantle velocity model. Additionally, the widespread existence of upper mantle anisotropy beneath the stations also mandates corrections before any D″ signature can be fully isolated. We therefore apply such upper mantle anisotropy corrections to the extent currently possible.

2. Data Set: *S-SKS* and *SV-SH* Differential Times

[5] We retrieve broadband digital data from 114 South American earthquakes with hypocentral depths greater than 100 km and magnitudes between 5.5 and 7.2. Our main sources of data are the Incorporated Research Institutions for Seismology (IRIS) and the Observatories and Research Facilities for European Seismology (ORPHEUS) data centers. Instrument responses are deconvolved from all data to obtain displacement traces that are then rotated to the great circle reference frame to obtain the horizontal plane longitudinal and transverse components. To further minimize possible *SV*-to-*P* contamination in the horizontal projection of the *SV* component, the vertical and longitudinal components were rotated into the reference frame of the incident ray path and wave front, to obtain "true" *SV* motion. The Preliminary Reference Earth Model (PREM) [*Dziewonski and Anderson*, 1981] was used to calculate the incidence angle beneath each station for this additional rotation. All data in the distance range 80°–130° were initially considered. Data with poor signal-to-noise ratio, complex earthquake source time functions, or possible arrival time picking errors of >1 s were not used in the study. These constraints resulted in 53 events and 1576 *SH* and *SV* pairs that were further analyzed. Only the highest-quality seismograms (clear impulsive phase onsets) were measured, yielding 306 record pairs from 28 earthquakes (Table 1) that were further evaluated for differential and splitting times.

[6] To avoid mapping the contaminating effects of upper mantle anisotropy to deep mantle structure in our data set, we evaluated potential sources of upper mantle anisotropy on both the source and receiver sides of ray paths. In general, upper mantle anisotropy likely persists to depths of 200–400 km, as suggested by mineral physics results [*Karato and Wu*, 1993] and corroborated by a host of seismic studies (i.e., reviews by *Silver* [1996] and *Savage* [1999, and references therein]), but may exist to greater depths, particularly in subduction zones [i.e., *Sharp et al.*, 1994; *Fouch and Fischer*, 1996; *Montagner*, 1998; *Kavner*, 2003; *Cordier et al.*, 2004]. For our data set, two potential upper mantle contaminants must be addressed: (1) within or near the subducting slab on the source side and (2) beneath the receiver.

[7] On the source side, anisotropy within or near the slab would produce gradually varying changes for a suite of downgoing ray paths recorded at a range of stations at similar azimuths. While upper mantle anisotropy has been observed in portions of our source areas [i.e., *Russo and Silver*, 1994; *Bock et al.*, 1998; *Polet et al.*, 2000], we do not observe these potential effects in our data set. More specifically, the pattern of weak to no splitting observed for deep focus events (e.g., 500 km and deeper) remains unchanged when including shallower events. We therefore rule out the possibility that source-side anisotropy is a major contributor to the overall character of shear wave splitting observed in our data set.

[8] To address the potential effects of receiver-side upper mantle anisotropy [e.g., *Silver*, 1996], we applied waveform corrections for most stations. In this correction, we rotated the great circle *SV* and *SH* components to the fast and slow polarization directions determined by these upper mantle studies (usually based on *SKS* arrivals), advanced the slow component in time by the value of the splitting time, and rotated the components back to the great circle reference frame. Unfortunately, many of the stations used in this study currently do not have published measurements of upper mantle anisotropy that can serve as the basis for upper mantle corrections. For some of these stations, we were able to obtain single-event shear wave splitting parameters by minimizing energy on the transverse component of *SKS* using the method of *Silver and Chan* [1991] and the error analysis method of *Fouch and Fischer* [1996]. In these cases (26 measurements for 14 stations), we applied our single station splitting model to the full waveform. For the remaining stations with no available corrections from either our own analyses or the published literature, the general lack of evidence for *SKS* splitting set allows us to proceed under the reasonable assumption that the absence of corrections for upper mantle anisotropy does not lead to a significant misinterpretation of D″ anisotropy for these stations.

[9] While it is likely that there is some difference in the effect of upper mantle anisotropy due to varying angles of incidence between *S* and *SKS*, these incidence angles typically differ by <10° and the effects are probably negligible. The typical assumption of horizontal hexagonal

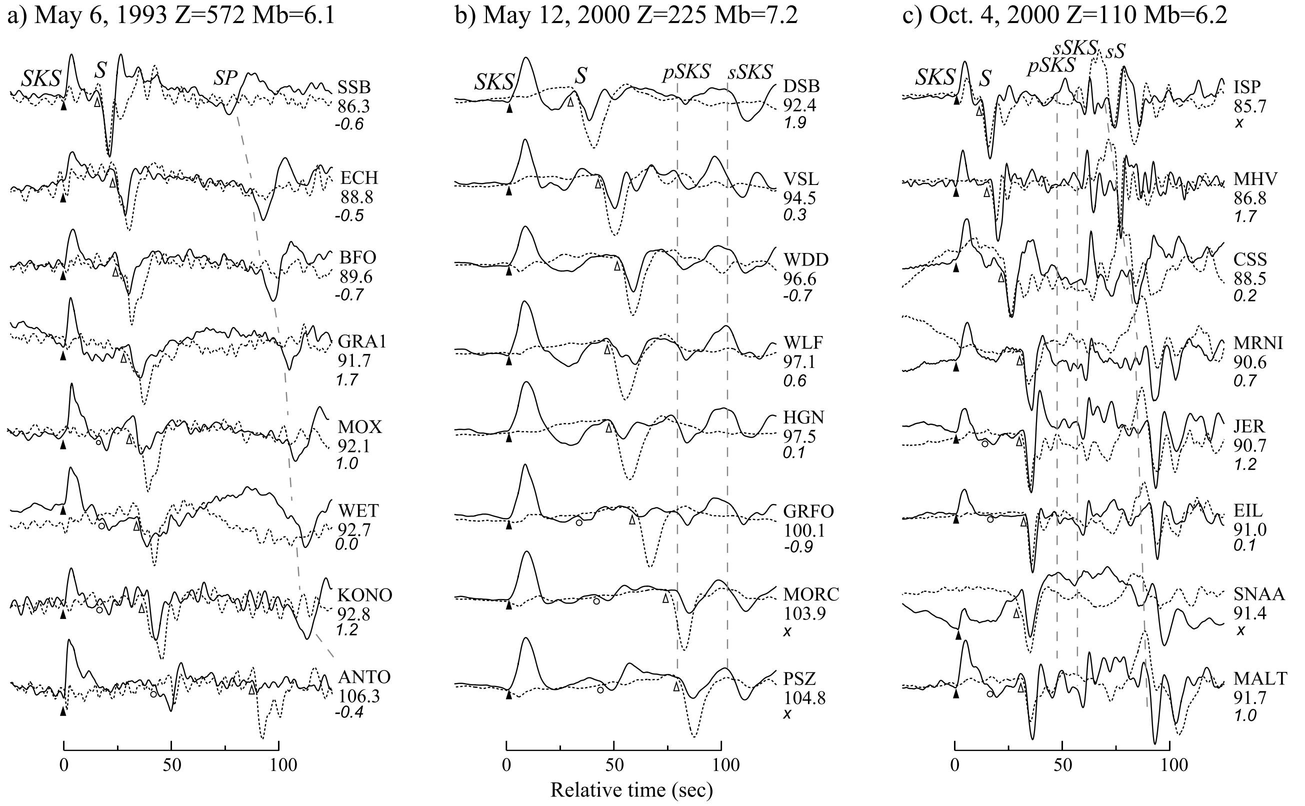

Figure 2. Radial (solid) and transverse (dotted) component displacement seismograms for three different deep focus South American earthquakes. All records are scaled in time to *SKS* and in amplitude to the largest arrival in the time window. *SKS* arrivals are noted by the solid triangles; the open triangles correspond to the *S* (or S_{diff}) arrivals, and the open circles indicate *SKKS*. Seismographic station names and epicentral distances (in degrees) are indicated to the right of each record pair. The difference in *SV* and *SH* (*SV-SH*, in s) is also indicated, where measurable; a cross indicates the measurement could not be made. Additional arrivals are also indicated.

symmetry axes underlying receiver anisotropy determinations is almost always too poorly constrained to justify correction for the associated incidence angle dependence. Additionally, while we recognize that single-event estimates are generally less well resolved relative to most published studies, we find that the overall waveform quality in *S* and S_{diff} is often improved using these corrections. Future work will involve generating improved or new upper mantle anisotropy corrections for these stations. Figure 2 shows broadband data from three typical earthquakes. These data are utilized for *S-SKS* differential travel time measurements (with *S* measured on the *SH* trace, *SKS* on *SV*) and *SV-SH* shear wave splitting of *S* (and S_{diff}). The data in Figure 2 display varying amounts of *SKS* energy leaking onto the tangential components: the May 6, 1993 event (column a) shows the most, while the other two events are fairly devoid of such leakage (except the first record in column c, which was excluded from further analysis. Generally, any record containing significant *SKS* energy on the *SH* component was discarded from our analyses, regardless of whether the station does or does not have a well-established upper mantle anisotropy correction. In the case of published corrections that fail to eliminate *SKS*(*SH*), and fail to linearize *SKS* particle motion, it is conceivable that deeper mantle anisotropy may be affecting *SKS* [e.g., *Hall et al.*, 2004]. It is also possible that the standard assumption of a horizontal hexagonal symmetry axis for the upper mantle anisotropy is incorrect, leading to an inadequate correction even for *SKS*. Failure of upper mantle anisotropy corrections to fully linearize the deep mantle phases of interest is actually common [e.g., *Garnero and Lay*, 1997]. Furthermore, the rapid amplitude decay of SV_{diff} with distance makes it difficult to appraise the effect of the receiver correction on the *S* phase. Thus we expect the associated uncertainty for differential travel time picks to be on the order of one second.

[10] All time picks in this study are made by hand picking phase onsets; only simple, impulsive arrivals are measured. While it is often desirable to use some form of waveform correlation method to obtain differential times [e.g., *Fouch et al.*, 2001], waveform variability in our data set is common, especially for SV_{diff}. Thus careful hand measurements were chosen as a more robust procedure for onset time determination. The measured *SV-SH* differential times are also included in Figure 2 (shown below the epicentral distance to the right of each trace). Most of these data have only minor splitting, which is representative of our entire data set. These same data are measured for the *S-SKS* times.

[11] To calculate *S-SKS* travel time residuals ($\delta T_{S\text{-}SKS}$), differential times predicted for PREM (the 1 Hz structure)

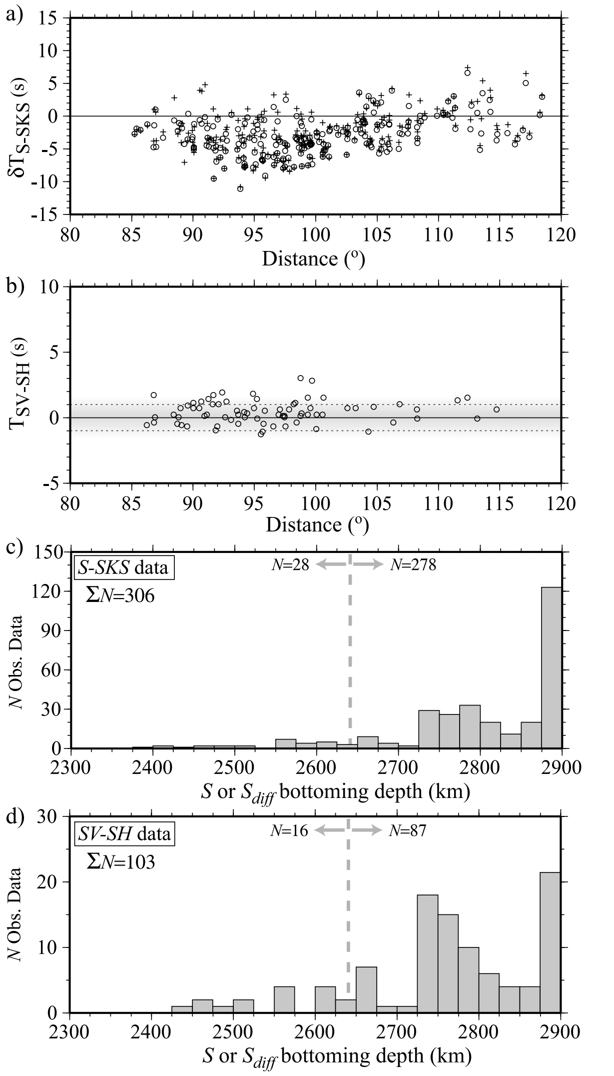

Figure 3. (a) Differential travel time residuals of *S-SKS* (observed differential time minus PREM predictions, notated as $\delta T_{S\text{-}SKS}$) versus distance. Residuals are plotted before (crosses) and after (circles) correction of aspherical mantle contributions above D″ as predicted by *Grand* [2002]. (b) Shear wave splitting measurements of all *S* data versus epicentral distance. The lightly shaded region in the ±1 s interval represents the level of possible picking error, and hence signals within this band may equally well be explained by essentially no split. Histograms of the number of data in PREM-predicted bottoming depth bins for the (c) *S-SKS* residuals and (d) *SV-SH* splits. The vertical dashed line corresponds to 250 km above the CMB.

were subtracted from observed differential times. We next compute aspherical mantle contributions above D″ for the differential times as predicted by the tomographic mantle shear velocity structure obtained by *Grand* [2002]. Contributions to *S* travel time perturbations are computed down to a depth of 250 km above the CMB, and throughout the whole mantle for *SKS*. This correction is intended to account for anomalously fast or slow velocity regions traversed in the shallow and midmantle that could contaminate our estimation of heterogeneity in D″. The corrected differential time data are plotted as a function of epicentral distance in Figure 3a. At any distance, the anomalies scatter over about 10 s, and display a slight trend with distance from a minimum near 95°, compatible with sampling somewhat higher-velocity material under the western Atlantic, transitioning to more PREM-like mantle in the east. The portions of the ray paths within the lower 250 km of the mantle are predominantly below the Atlantic (Figure 1c). Our data clearly provide very little azimuthal sampling at the ray path bottoming depths.

[12] The shear wave splitting measurements are also plotted against distance (Figure 3b). With *SV-SH* measurement error possibly as large as ±1 s, this range is shaded in the figure; nearly 75% of all *SV-SH* measurements fall within this range. This observation is in contrast to other regions which commonly result in S_{diff} splitting in the 2–6 s range, for example, beneath the Pacific [e.g., *Ritsema et al.*, 1998; *Vinnik et al.*, 1998; *Fouch et al.*, 2001] and beneath the Caribbean [e.g., *Kendall and Silver*, 1996; *Garnero and Lay*, 2003]. The number of data as a function of computed *S* wave bottoming depths for the *S-SKS* and *SV-SH* measurements is shown in Figures 3c and 3d, respectively. A significant number of the data are predicted to turn in the lowermost 250 km of the mantle (dashed line); these data will be exploited in section 3 to infer D″ heterogeneity and anisotropy.

[13] In addition to our *S-SKS* and *SV-SH* measurements on broadband recordings, measurements were also made on the same data after low-pass filtering with a corner of 0.1 Hz. The motivation for this exercise was to assess consistency between the broadband (BB) and low-passed (LP) data, with the hope that slightly noisy data that would otherwise be discarded might prove usable. Figure 4 compares the BB and LP measurements for *S-SKS* residuals and *SV-SH* splits. In general, the *S-SKS* measurements display fairly good agreement, though with some scatter. The *SV-SH* measurements show several cases of significant disagreement between the BB and LP measurements. This is predominantly due to a larger picking error for the LP records, especially for the SV_{diff} phase, which is routinely the weakest arrival measured. We therefore discard all LP *SV-SH* measurements. However, 29 LP *S-SKS* measurements were retained for records when the BB channel could not be measured with confidence. This amounts to just over 10% of our

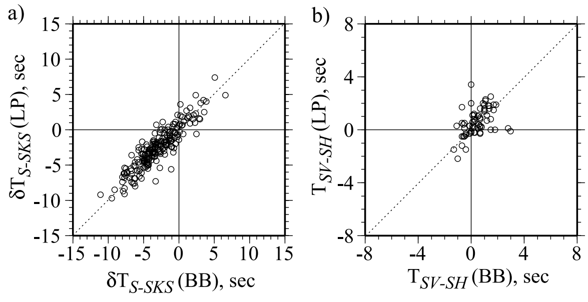

Figure 4. (a) *S-SKS* residuals and (b) *SV-SH* splitting is compared for measurements on broadband (BB) recordings and their low-pass filtered equivalents (LP) with a corner frequency of 0.1 Hz.

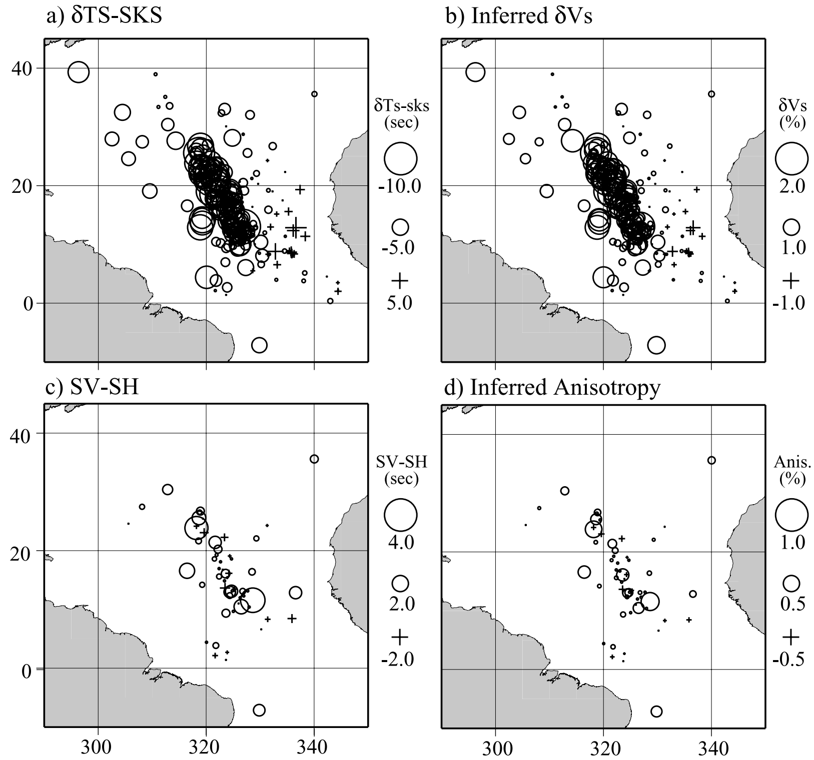

Figure 5. (a) The $\delta T_{S\text{-}SKS}$ residuals plotted at path midpoints. (b) Path-averaged shear velocity anomaly estimates for D″ beneath the Atlantic plotted at ray path midpoints. Values are in percent velocity perturbations. (c) Raw *SV-SH* times plotted at path midpoints and (d) resulting D″ anisotropy inferred from mapping splits into PREM predicted D″ path lengths. The predominance of relatively minor splitting is apparent.

BB *S-SKS* data set. Only the highest-quality seismograms (clear impulsive phase onsets) were measured, yielding 306 record pairs from 28 earthquakes (Table 1) that were further evaluated for differential and splitting times (also see auxiliary material[1]).

3. Inferring Seismic Heterogeneity and Anisotropy in D″

[14] D″ shear velocity heterogeneity is mapped using a D″ reference velocity structure (in this case, PREM), an estimate of ray path length in D″ based on ray tracing in that structure assuming a 250 km thickness of D″, and the corrected differential travel time residual being is attributed to the *S* path in D″. This allows us to compute D″ path-averaged velocity anomalies relative to PREM for each datum. The aspherical model-corrected *S-SKS* differential time residuals and those converted into D″ δV_S estimates are shown in Figures 5a and 5b, respectively. Differential times and velocity anomalies are plotted at the D″ path midpoints. The coverage is densest in the center of the Atlantic, between 10° and 30° latitude. For our assumed D″ thickness of 250 km, the individual path shear velocity anomalies range between −1% and +2% (Figure 5b) with a trend from higher velocity to lower velocity moving toward the east/southeast under the Atlantic. This spatial trend agrees well with a large-scale lowermost mantle transition across the Atlantic found in tomographic models [e.g., *Su et al.*, 1994; *Megnin and Romanowicz*, 2000; *Masters et al.*, 2000; *Grand*, 2002].

[15] It is important to note that this method of inferring heterogeneity distributes the travel time anomaly along the entire path segment in D″ (Figure 1c) so that the emergence of the strong small-scale variation seen in Figure 5b must reflect a rather acute lateral gradient in the structure. It is plausible that the velocity gradient is quite abrupt and strong, but our path coverage is insufficient to uniquely resolve it, while the global tomography models are heavily smoothed so that this region would be averaged to near-zero anomaly. The most densely sampled part of our study has δV_S between 1 and 1.5%. This is in contrast to the regions of anisotropy studies noted above, which contain some of the lowest or highest D″ velocities on Earth.

[16] To characterize anisotropy in D″ beneath the Atlantic, the *SV-SH* shear wave splitting measurements for those *S* waves predicted to bottom within the lowermost 250 km of the mantle (according to the PREM model) are used. This measurement is made for the onsets of arrivals, which is a valid measure of splitting only if the underlying assumption that any D″ anisotropy has a symmetry orientation that allows *SV* and *SH* to decouple. This assumption, which is valid for grazing incidence in VTI material, is not tightly constrained, as we discuss in the next section. However, it allows us to assess first-order geographical trends in split-

[1]Auxiliary material is available at ftp://ftp.agu.org/apend/jb/2004JB003004.

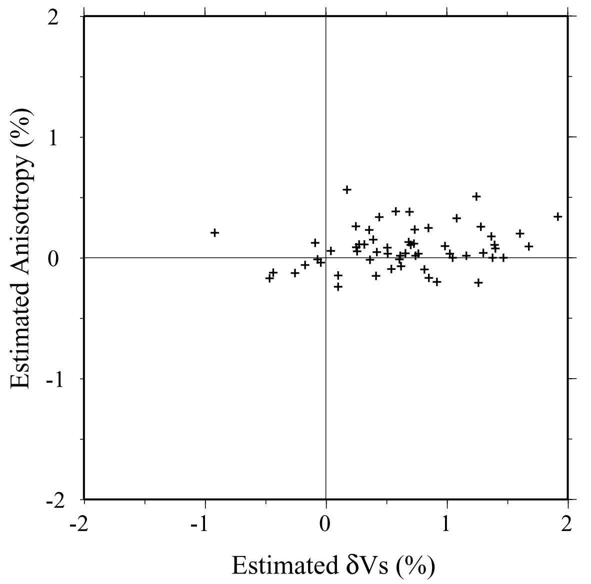

Figure 6. Comparison of estimated shear wave anisotropy and heterogeneity (δV_S) for records that provided both *S-SKS* and *SV-SH* measurements. See text for more details.

ting and inferred anisotropy if VTI is the appropriate mechanism, as suggested for other regions of D″. The PREM-predicted D″ path lengths are used along with splitting times to infer anisotropy strength. The raw splitting times and resulting anisotropy are shown plotted at D″ path midpoints in Figures 5c and 5d, respectively. This sampling is not as dense as for our shear velocity heterogeneity measurements, but the central part of the Atlantic has ample measurements. A primary finding of this paper is the widespread predominance of either isotropy or, at most, weak VTI anisotropy in the lowermost mantle beneath the Atlantic. The majority of our anisotropy estimates are within ±0.5%.

[17] For waveforms that provide both *S-SKS* and *SV-SH* times, anisotropy and heterogeneity estimates are directly compared in Figure 6. There is no apparent correlation, primarily as a result of the anisotropy estimates being essentially zero or within the measurement error. *Garnero and Lay* [2003] found a mild correlation between anisotropy and heterogeneity beneath the Caribbean, a region that contains significant strength in the associated patterns. Very similar correlation was established on a localized scale beneath the Cocos Plate by *Rokosky et al.* [2004].

4. Anisotropy Geometry Uncertainties

[18] Most prior studies of D″ anisotropy observe a predominance of *SV* delays relative to *SH* for *S*, S_{diff}, or *ScS* [see, e.g., *Moore et al.*, 2004]. Relative delay of *SV* for horizontally propagating ray paths is compatible with VTI being the dominant orientation for D″ anisotropy (see reviews by *Wysession et al.* [1998], *Lay et al.* [1998a, 1998b], and *Kendall* [2000]). Even for the fewer cases where *SV* has been observed to be early relative to *SH*, it appears that the two components are usually decoupled [e.g., *Pulliam and Sen*, 1998; *Russell et al.*, 1998, 1999]. It is possible, of course, that azimuthal anisotropy is present, in which case there will not generally be a decoupling of the *SV* and *SH* phases (i.e., no relative shifting of their onset times). Instead, we would expect a mixing of fast and slow phases onto both the *SH* and *SV* components. This effect can result in waveform complexity and waveshape dependence on the initial *S* wave polarization [e.g., *Garnero et al.*, 2003]. Most of the *S* waves used in our *SV-SH* measurements have fairly simple waveforms, although the background noise level is often appreciable (e.g., see Figure 2), which allows us to explore some data attributes that might indicate the presence of azimuthal anisotropy.

[19] Particle motion analyses that identify deviation from linear S polarization are commonly an integral part of upper mantle anisotropy studies. However, beyond 90°, *S* waves are not expected to have linear particle motion, even for an isotropic lower mantle velocity structure. At these distances, the converging *S* and *ScS* phases are oppositely polarized on the *SV* component, but have the same polarity on the *SH* component of motion, with differences between resulting destructive and constructive interference near the onset of diffraction causing nonlinear particle motion. This tends to make *SV* waveforms narrower than their *SH* counterparts near the core shadow, with rapid amplitude decay of *SV* as a function of distance [e.g., *Lay and Young*, 1991]. Simple polarization analysis is therefore not reliable in this case. In an azimuthally anisotropic medium the coupling of fast and slow waves into *SV* and *SH* polarizations will modify the waveform behavior as diffractions initiates. By assessing the waveform stability and evolution with distance for numerous events with diverse radiation patterns (and hence variable *S* polarization vectors entering into the D″ portion of the propagation paths), we can assess whether there is evidence for strong coupling of the *SH* and *SV* components that might favor azimuthal anisotropy. Persistence of *SV* amplitudes for large distances into the core shadow requires either strong negative gradients in the velocity structure above the CMB that delay or prevent the onset of diffraction [e.g., *Ritsema et al.*, 1997] or strong coupling between *SH* and *SV* components due to diffraction in azimuthally anisotropic material [e.g., *Vinnik et al.*, 1998]. In our data, rapid amplitude decay of *SV* with distance is regularly observed beyond about 97° (as apparent in Figure 2b), which does not argue in favor of either of the latter two possibilities. The observed *SV* amplitude decay is instead compatible with isotropic behavior, or with decoupled anisotropic (VTI) behavior [see *Lay and Young*, 1991].

[20] Another assessment of possible *SV* and *SH* coupling is to search for dependence of the observed *SV* amplitudes on those of *SH*, as would be expected for strongly coupled behavior in the presence of azimuthal anisotropy [e.g., *Vinnik et al.*, 1995, 1998]. Figure 7 presents the amplitude behavior of *SV* for our data set. Many *SV* signals are quite small and have variable waveforms as the core shadow distance is approached. We therefore compute envelopes for the windowed *SV* pulse, with the envelope instantaneous peak amplitude being used for robust *SV* amplitude measurement. These values are referenced to *SKKS* amplitudes, because *SKKS* is close in incidence angle at the station and usually similar in radiation pattern at the source. Figure 7a shows the behavior with distance of the *SV*/*SKKS* ratio. At the closer distances, *SKKS* is just emerging, so it is

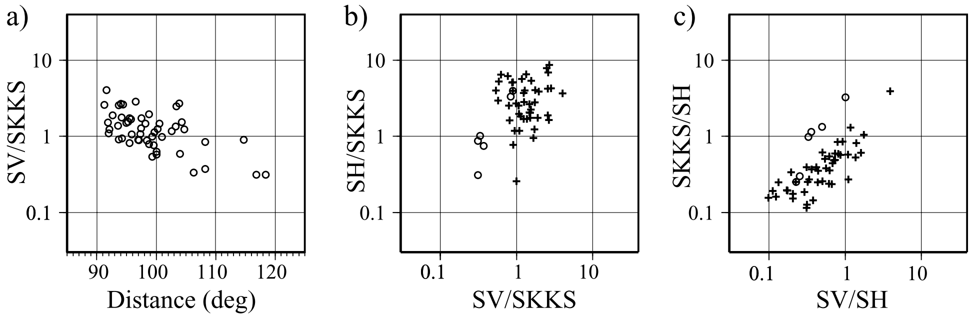

Figure 7. Comparison of various *SV* amplitude ratios, as measured from the envelope of the phase of interest: (a) *SV* referenced to *SKKS* is shown as a function of epicentral distance. (b) Plots of *SV* and *SH*, using *SKKS* as a reference. Circles and crosses are for data at distances greater and less than 105°, respectively. (c) *SV* and *SKKS* plotted using *SH* as a reference. Circles and crosses as in Figure 7b.

relatively weak, while *SV* is strong. At the larger distances; the opposite is true, as can be seen from the general trend of *SV/SKKS* reducing with distance (there is considerable scatter). Unfortunately, for this source-receiver geometry, the strong *SV* amplitude decay at large distances results in only a few measurements beyond 105°, where *SKKS* is fully developed and stable. Nonetheless, we compare *SV* to *SH* with each normalized by *SKKS* in Figure 7b. The data at distances larger than 105° are the circles, and the closer distance observations are crosses. Taken as a whole data set (i.e., the whole distance range), there is a slight suggestion of a positive correlation of *SV* and *SH*. However, the concentration of data at distances where *SKKS* is not particularly strong makes this assessment suspect, and in fact the corresponding data plot as a cloud of points. Another approach is to compare *SV* and *SKKS*, both being normalized by *SH*: a positive correlation would suggest that there is not strong *SV-SH* coupling since *SKKS* should be independent of *SH*. Figure 7c shows that a positive correlation between *SKKS*/*SH* and *SV*/*SH* is suggested in our data set. This suggests the possibility that the weak correlations between *SV* and *SH* amplitudes in Figure 7 may be fortuitous, resulting from focal mechanism systematics. Figure 7 highlights the difficulty in constraining anisotropy orientation in the face of the weakening of the important SV_{diff} phase with epicentral distance near the edge of the core shadow zone.

[21] This study, like all previous studies of D″ anisotropy, has almost no azimuthal coverage of the region sampled, which intrinsically precludes placing tight spatial constraints on the vertical and lateral location of anisotropy, and limits our ability to constrain the symmetry axis for any anisotropy that is present. Given the limited azimuthal coverage, it is possible that we may misinterpret the extent of any azimuthal anisotropy due to sampling a degenerate azimuth that does not give much splitting. In other words, the absence of large shifts between *SV* and *SH* onset times bounds the amount of VTI that may be present but does not itself preclude even strong azimuthal anisotropy from being present. It is also possible that small-scale heterogeneity in the anisotropic boundary layer could be confused or unresolved given the relatively long paths involved in *S* or S_{diff} data. These concerns make it difficult to make definitive interpretations of the region, but there is no question that this region differs from others that have been investigated, most of which have stronger VTI, and the simplest interpretation of the present data is that the level of anisotropy is significantly weaker relative to that in previously studied regions.

5. Interpretation

[22] As stated above, uncertainties exist in mapping *S* wave splits to definitive models of anisotropy. Nonetheless, it is instructive to further quantify the VTI end-member case for our data, for comparison with other regions. Figure 8 displays the *SV-SH* times of Figure 3b (circles) compared to predictions from reflectivity synthetic seismograms [e.g., *Müller*, 1985] for various VTI models, where the predictions (lines) have been measured exactly as in the data. Again, the shaded region brackets *SV-SH* shifts within ±1 s, since this is the maximum projected measurement error. The data are also coded according to source depth, since it is possible that near-source anisotropy may contribute to (contaminate) our measurements for shallower events. The possibility that source-side mantle anisotropy [e.g., *Russo and Silver*, 1994; *Fouch and Fischer*, 1996; *Wookey et al.*, 2002] may be contributing is suggested by the slightly larger scatter of *SV-SH* times for event depths <300 km. However, the general trend with distance for the different source depths appears robustly averaged near or just about zero: a least squares fit to all data suggests a slight increase in splitting time with distance, though the average is quite small. Four VTI models are shown: 100 or 300 km thick layers containing 0.5 or 1.0% uniform VTI. The two different VTI zone thicknesses are considered to emphasize the trade-offs involved for modeling assumptions [see also *Garnero and Lay*, 1998]. While 0.5–1.0% VTI distributed uniformly over 300 km of the lowermost mantle is too strong, lower values of 0.25% or less would fit the average trend of the data. Or conversely, reducing the thickness of the VTI zone can also fit this trend, such as 0.5% VTI in 100 km of the lowermost mantle. This range agrees well with the predictions from anisotropy strength derived from splitting times and D″ path length estimates (Figure 5d), probably owing to the PREM reference structure being appropriate for the central Atlantic.

[23] Combined with the overall low level of velocity heterogeneity observed for this region, the relatively low level and/or absence of shear wave splitting raises some

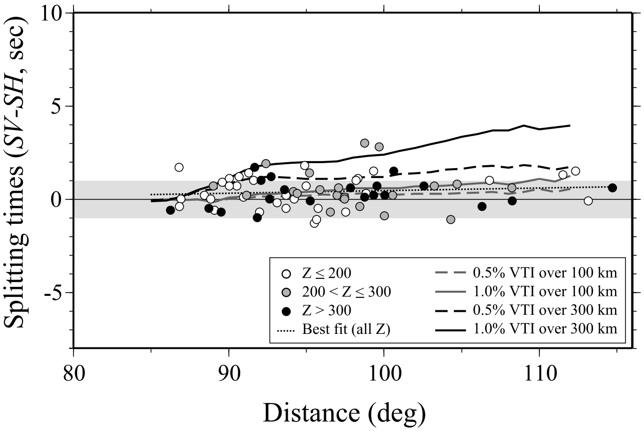

Figure 8. Observed shear wave splitting demarked for different source depth intervals (Z, in km), and a least squares fit to all the splits (thin dotted line). Also shown are predicted splits for different models containing vertical axis of symmetry transverse isotropy (VTI). The shaded region corresponds to *SV-SH* times within ±1 s, which represents the magnitude of possible picking error.

interesting possibilities about the nature of D″ anisotropy. Two explanations for the origin of seismic anisotropy in the deep mantle are commonly considered: lattice preferred orientation (LPO) of mantle mineral, or shape preferred orientation (SPO) of deep mantle structures. It has been suggested that LPO, possibly in the MgO minerals of the deep mantle, dominates in areas of subduction, where high stresses and relatively low temperatures due to the subducting slab preferentially orientates crystals by dislocation creep [e.g., *McNamara et al.*, 2002]. This could account for circum-Pacific regions of D″ being well modeled with a VTI anisotropy mechanism. SPO has been proposed to dominate beneath (or within) areas of upwelling, in which chemical heterogeneities or possibly melt inclusions are oriented by shear flows to produce an anisotropic fabric [e.g., *Russell et al.*, 1999; *Kendall*, 2000; *Fouch et al.*, 2001]. On the basis of the regional shear velocity values, the deep mantle beneath the central Atlantic may be transitional between high-velocity, relatively cooled regions with subduction-related LPO (beneath the Americas [e.g., *Kendall and Silver*, 1996, 1998; *Garnero and Lay*, 2003]) and low-velocity, relatively warm regions of upwelling-related SPO (beneath Africa to the east/southeast, where a superplume has been imaged [e.g., *Ni and Helmberger*, 2003]). We postulate that strong deep mantle anisotropy is most easily detectable in regions having strong midmantle flow-related velocity heterogeneity. The mantle under the central Atlantic has low-heterogeneity amplitudes and has not experienced any recent subduction, nor does it appear to be associated with significant upwelling. Thus a plausible explanation for the lack of anisotropy in the region is that there is deficient magnitude of strain (and possibly not low enough temperatures) needed for LPO to develop, and there are not strong enough shear flows to align chemical heterogeneities or partial melts to develop SPO. This opens up the possibility of using the variability in magnitude of D″ anisotropy to place constraints on dynamical processes affecting the boundary layer.

6. Conclusions

[24] Using *S-SKS* differential time residuals, the lowermost mantle beneath the central Atlantic is found to have low-to-moderate shear velocity heterogeneity with base levels close to average Earth models, consistent with tomographic models. Quite low levels of *SV-SH* shear wave splitting are also observed for this same region. When mapping the anisotropy with a VTI geometry, a widespread predominance of weak (or absent) lowermost mantle anisotropy (−0.5% to +0.5%) is found beneath the Atlantic. The lack of anisotropy in this region of D″ is in contrast to other study areas, such as beneath the Caribbean, Alaska, or the central Pacific, each which have more significant inferred levels of D″ anisotropy (e.g., up to 2%) and stronger regional velocity deviations from reference models (±3%). Unlike these areas, the lowermost mantle beneath the Atlantic may lack conditions necessary to produce D″ anisotropy, such as large-scale mantle downwellings or upwellings which give rise to the temperature and stress conditions that can generate LPO or SPO.

[25] **Acknowledgments.** We would like to thank Jim Tyburczy for helpful comments, Chad Trabant for help with European data gathering, and IRIS and ORPHEUS data centers for supplying the broadband data used in this study. Most figures were made using Generic Mapping Tools [*Wessel and Smith*, 1991]. This research was supported by NSF grants EAR-9996302 (E.G., M.M.) and EAR-0125595 (T.L.).

References

Bock, G., R. Kind, A. Rudloff, and G. Asch (1998), Shear wave anisotropy in the upper mantle beneath the Nazca plate in northern Chile, *J. Geophys. Res.*, *103*, 24,333–24,345.
Bullen, K. E. (1949), Compressibility-pressure hypothesis and the Earth's interior, *Mon. Not. R. Astron. Soc. Geophys. Suppl.*, *5*, 355–368.
Cordier, P., T. Ungar, L. Zsoldos, and G. Tichy (2004), Dislocation creep in $MgSiO_3$ perovskite at conditions of the Earth's uppermost lower mantle, *Nature*, *428*, 837–840.
Ding, X. M., and D. V. Helmberger (1997), Modeling D″ structure beneath Central America with broadband seismic data, *Phys. Earth Planet. Inter.*, *101*, 245–270.
Dziewonski, A. M., and D. L. Anderson (1981), Preliminary reference Earth model, *Phys. Earth Planet. Inter.*, *25*, 297–356.
Fouch, M. J., and K. M. Fischer (1996), Mantle anisotropy beneath northwest Pacific subduction zones, *J. Geophys. Res.*, *101*, 15,987–16,002.
Fouch, M. J., K. M. Fischer, and M. E. Wysession (2001), Lowermost mantle anisotropy beneath the Pacific: Imaging the source of the Hawaiian plume, *Earth Planet. Sci. Lett.*, *190*(3–4), 167–180.
Garnero, E. J. (2000), Heterogeneity of the lowermost mantle, *Annu. Rev. Earth Planet. Sci.*, *28*, 509–537.
Garnero, E. J., and T. Lay (1997), Lateral variations in lowermost mantle shear wave anisotropy beneath the North Pacific and Alaska, *J. Geophys. Res.*, *102*, 8121–8135.
Garnero, E. J., and T. Lay (1998), Effects of D″ anisotropy on seismic velocity models of the outermost core, *Geophys. Res. Lett.*, *25*, 2341–2344.
Garnero, E. J., and T. Lay (2003), D″ shear velocity heterogeneity, anisotropy and discontinuity structure beneath the Caribbean and Central America, *Phys. Earth Planet. Inter.*, *140*, 219–242.
Garnero, E. J., V. Maupin, T. Lay, and M. J. Fouch (2003), Complexities in D″ anisotropy beneath the Caribbean: Evidence for a tilted symmetry axis of transversely isotropic media from data and synthetics, *Eos Trans. AGU*, *84*(46), Fall Meet. Suppl., Abstract U51B-0007.
Grand, S. P. (2002), Mantle shear-wave tomography and the fate of subducted slabs, *Philos. Trans. R. Soc. London, Ser. A*, *360*(1800), 2475–2491.
Grand, S. P., R. D. van der Hilst, and S. Widiyantoro (1997), Global seismic tomography: A snapshot of convection in the Earth, *GSA Today*, *7*, 1–7.

Hager, B. H., R. W. Clayton, M. A. Richards, R. P. Comer, and A. M. Dziewonski (1985), Lower mantle heterogeneity, dynamic topography and the geoid, *Nature*, *313*, 541–546.
Hall, S. A., M. van der Baan, and J.-M. Kendall (2004), Some comments on the effects of lower-mantle anisotropy on *SKS* and *SKKS* phases, *Phys. Earth. Planet Inter.*, in press.
Jellinek, A. M., and M. Manga (2004), Links between long-lived hotspots, mantle plumes, D″, and plate tectonics, *Rev. Geophys.*, *42*, doi:10.1029/2003RG000144, in press.
Karato, S. (1998), Some remarks on the origin of seismic anisotropy in the D″ layer, *Earth Planets Space*, *50*(11–12), 1019–1028.
Karato, S. (2003), *The Dynamic Structure of the Deep Earth: An Interdisciplinary Approach*, 241 pp., Princeton Univ. Press, Princeton, N. J.
Karato, S., and B. B. Karki (2001), Origin of lateral variation of seismic wave velocities and density in the deep mantle, *J. Geophys. Res.*, *106*, 21,771–21,783.
Karato, S.-I., and P. Wu (1993), Rheology of the upper mantle: A synthesis, *Science*, *260*, 771–778.
Kavner, A. (2003), Elasticity and strength of hydrous ringwoodite at high pressure, *Earth Planet. Sci. Lett.*, *214*(3–4), 645–654.
Kendall, J.-M. (2000), Seismic anisotropy in the boundary layers of the mantle, in *Earth's Deep Interior: Mineral Physics and Tomography From the Atomic to the Global Scale*, *Geophys. Monogr. Ser.*, vol. 117, edited by S. Karato et al., pp. 133–159, AGU, Washington, D. C.
Kendall, J.-M., and P. M. Shearer (1995), On the structure of the lowermost mantle beneath the Southwest Pacific, Southeast-Asia and Australasia, *Phys. Earth Planet. Inter.*, *92*, 85–98.
Kendall, J.-M., and P. G. Silver (1996), Constraints from seismic anisotropy on the nature of the lowermost mantle, *Nature*, *381*, 409–412.
Kendall, J.-M., and P. G. Silver (1998), Investigating causes of D″ anisotropy, in *The Core-Mantle Boundary Region*, *Geodyn. Ser.*, vol. 28, edited by M. Gurnis et al., pp. 97–118, AGU, Washington, D. C.
Lay, T., and E. J. Garnero (2004), Core-mantle boundary structures and processes, in *Geophysical Monograph Series*, edited by S. Sparks and C. Hawkesworth, AGU, Washington, D. C., in press.
Lay, T., and D. V. Helmberger (1983), The shear wave velocity gradient at the base of the mantle, *J. Geophys. Res.*, *88*, 8160–8170.
Lay, T., and C. J. Young (1990), The stably-stratified outermost core revisited, *Geophys. Res. Lett.*, *17*, 2001–2004.
Lay, T., and C. J. Young (1991), Analysis of seismic *SV* waves in the core's penumbra, *Geophys. Res. Lett.*, *18*, 1373–1376.
Lay, T., Q. Williams, and E. J. Garnero (1998a), The core-mantle boundary layer and deep Earth dynamics, *Nature*, *392*, 461–468.
Lay, T., Q. Williams, E. J. Garnero, L. Kellogg, and M. E. Wysession (1998b), Seismic wave anisotropy in the D″ region and its implications, in *The Core-Mantle Boundary Region*, *Geodyn. Ser.*, vol. 28, edited by M. Gurnis et al., pp. 229–318, AGU, Washington D. C.
Lay, T., E. J. Garnero, and Q. Williams (2004), Partial melting of a thermochemical boundary layer at the base of the mantle, *Phys. Earth Planet. Inter.*, in press.
Masters, G., G. Laske, H. Bolton, and A. Dziewonski (2000), The relative behavior of shear velocity, bulk sound speed, and compressional velocity in the mantle: Implications for chemical and thermal structure, in *Earths' Deep Interior: Mineral Physics and Tomography From the Atomic to the Global Scale*, *Geophys. Monogr. Ser.*, vol. 117, edited by S. Karato et al., pp. 63–87, AGU, Washington, D. C.
Matzel, E., M. K. Sen, and S. P. Grand (1996), Evidence for anisotropy in the deep mantle beneath Alaska, *Geophys. Res. Lett.*, *23*, 2417–2420.
McNamara, A. K., P. E. van Keken, and S. I. Karato (2002), Development of anisotropic structure in the Earth's lower mantle by solid-state convection, *Nature*, *416*, 310–314.
Megnin, C., and B. Romanowicz (2000), The three-dimensional shear velocity structure of the mantle from the inversion of body, surface and higher-mode waveforms, *Geophys. J. Int.*, *143*(3), 709–728.
Mitchell, B. J., and D. V. Helmberger (1973), Shear velocities at base of mantle from observations of *S* and *ScS*, *J. Geophys. Res.*, *78*, 6009–6020.
Montagner, J. P. (1998), Where can seismic anisotropy be detected in the Earth's mantle? In boundary layers.., *Pure Appl. Geophys.*, *151*(2–4), 223–256.
Moore, M. M., E. J. Garnero, T. Lay, and Q. Williams (2004), Shear wave splitting and waveform complexity for lowermost mantle structures with low-velocity lamellae and transverse isotropy, *J. Geophys. Res.*, *109*, B02319, doi:10.1029/2003JB002546.
Morgan, W. J. (1971), Convection plumes in the lower mantle, *Nature*, *230*, 42–43.
Müller, G. (1985), The reflectivity method: A tutorial, *J. Geophys.*, *58*, 153–174.
Ni, S. D., and D. V. Helmberger (2003), Seismological constraints on the South African superplume: Could be the oldest distinct structure on Earth, *Earth Planet. Sci. Lett.*, *206*(1–2), 119–131.
Polet, J., P. G. Silver, S. L. Beck, T. Wallace, G. Zandt, S. Ruppert, R. Kind, and A. Rudloff (2000), Shear wave anisotropy beneath the Andes from the BANJO, SEDA, and PISCO experiments, *J. Geophys. Res.*, *105*, 6287–6304.
Pulliam, J., and M. K. Sen (1998), Seismic anisotropy in the core-mantle transition zone, *Geophys. J. Int.*, *135*(1), 113–128.
Ribe, N. M., and D. P. Devalpine (1994), The global hotspot distribution and instability of D″, *Geophys. Res. Lett.*, *21*, 1507–1510.
Ritsema, J. (2000), Evidence for shear velocity anisotropy in the lowermost mantle beneath the Indian Ocean, *Geophys. Res. Lett.*, *27*, 1041–1044.
Ritsema, J., E. Garnero, and T. Lay (1997), A strongly negative shear velocity gradient and lateral variability in the lowermost mantle beneath the Pacific, *J. Geophys. Res.*, *102*, 20,395–20,411.
Ritsema, J., T. Lay, E. J. Garnero, and H. Benz (1998), Seismic anisotropy in the lowermost mantle beneath the Pacific, *Geophys. Res. Lett.*, *25*, 1229–1232.
Rokosky, J. M., T. Lay, E. J. Garnero, and S. A. Russell (2004), High-resolution investigation of shear-wave anisotropy in D″ beneath the Cocos Plate, *Geophys. Res. Lett.*, *31*, L07605, doi:10.1029/2003GL018902.
Russell, S. A., T. Lay, and E. J. Garnero (1998), Seismic evidence for small-scale dynamics in the lowermost mantle at the root of the Hawaiian hotspot, *Nature*, *396*, 255–258.
Russell, S. A., T. Lay, and E. J. Garnero (1999), Small-scale lateral shear velocity and anisotropy heterogeneity near the core-mantle boundary beneath the central Pacific imaged using broadband *ScS* waves, *J. Geophys. Res.*, *104*, 13,183–13,199.
Russo, R. M., and P. G. Silver (1994), Trench-parallel flow beneath the Nazca plate from seismic anisotropy, *Science*, *263*, 1105–1111.
Savage, M. K. (1999), Seismic anisotropy and mantle deformation; what have we learned from shear wave splitting?, *Rev. Geophys.*, *37*(1), 65–106.
Sharp, T. G., G. Y. A. Bussod, and T. Katsura (1994), Microstructures in b-$Mg_{1.8}Fe_{0.2}SiO_4$ experimentally deformed at transition-zone conditions, *Phys. Earth Planet. Inter.*, *86*, 69–83.
Silver, P. G. (1996), Seismic anisotropy beneath the continents: Probing the depths of geology, *Annu. Rev. Earth Planet. Sci.*, *24*, 385–432.
Silver, P. G., and W. W. Chan (1991), Shear wave splitting and subcontinental mantle deformation, *J. Geophys. Res.*, *96*, 16,429–16,454.
Su, W. J., R. L. Woodward, and A. M. Dziewonski (1994), Degree-12 model of shear velocity heterogeneity in the mantle, *J. Geophys. Res.*, *99*, 6945–6980.
Thomas, C., and J.-M. Kendall (2002), The lowermost mantle beneath northern Asia - II. Evidence for lower-mantle anisotropy, *Geophys. J. Int.*, *151*(1), 296–308.
Thomas, C., J.-M. Kendall, and M. Weber (2002), The lowermost mantle beneath northern Asia - I. Multi-azimuth studies of a D″ heterogeneity, *Geophys. J. Int.*, *151*(1), 279–295.
Thorne, M., E. J. Garnero, and S. Grand (2004), Geographic correlation between hot spots and deep mantle lateral shear-wave velocity gradients, *Phys. Earth Planet. Inter.*, *146*, 47–63.
Vinnik, L., B. Romanowicz, Y. Lestunff, and L. Makeyeva (1995), Seismic anisotropy in the D″ layer, *Geophys. Res. Lett.*, *22*, 1657–1660.
Vinnik, L., L. Breger, and B. Romanowicz (1998), Anisotropic structures at the base of the Earth's mantle, *Nature*, *393*, 564–567.
Wessel, P., and W. H. F. Smith (1991), Free software helps map and display data, *Eos Trans. AGU*, *72*, 441, 445–446.
Wookey, J., J.-M. Kendall, and G. Barruol (2002), Mid-mantle deformation inferred from seismic anisotropy, *Nature*, *415*, 777–780.
Wysession, M. E., T. Lay, J. Revenaugh, Q. Williams, E. J. Garnero, R. Jeanloz, and L. Kellogg (1998), The D″ discontinuity and its implications, in *The Core-Mantle Boundary Region*, *Geodyn. Ser.*, vol. 28, edited by M. Gurnis et al., pp. 273–298, AGU, Washington, D. C.

M. J. Fouch, E. J. Garnero, and M. M. Moore, Department of Geological Sciences, Arizona State University, Box 871404, Tempe, AZ 85287-1404, USA. (fouch@asu.edu; garnero@asu.edu; earthfireh2oair@yahoo.com)

T. Lay, Earth Sciences Department, University of California, Earth Marine Sciences Bldg., Santa Cruz, CA 95064, USA. (tlay@es.ucsc.edu)